15 Jul 2024

Kinetic Characterization and Identification of Key Active Site Residues of the L-Aspartate N-Hydroxylase, CreE

Sydney B. Johnson

Hannah Valentino

Pablo Sobrado
Missouri University of Science and Technology, psobrado@mst.edu

Recommended Citation

S. B. Johnson et al., "Kinetic Characterization and Identification of Key Active Site Residues of the L-Aspartate N-Hydroxylase, CreE," *ChemBioChem*, vol. 25, no. 14, article no. e202400350, Wiley; Wiley-VCH Verlag, Jul 2024.
The definitive version is available at https://doi.org/10.1002/cbic.202400350

ChemBioChem

Research Article
doi.org/10.1002/cbic.202400350

Chemistry Europe
European Chemical Societies Publishing

www.chembiochem.org

Kinetic Characterization and Identification of Key Active Site Residues of the L-Aspartate *N*-Hydroxylase, CreE

Sydney B. Johnson,[a] Hannah Valentino,[a] and Pablo Sobrado*[a, b]

CreE is a flavin-dependent monooxygenase (FMO) that catalyzes three sequential nitrogen oxidation reactions of L-aspartate to produce nitrosuccinate, contributing to the biosynthesis of the antimicrobial and antiproliferative nautral product, cremeomycin. This compound contains a highly reactive diazo functional group for which the reaction of CreE is essential to its formation. Nitro and diazo functional groups can serve as potent electrophiles, important in some challenging nucleophilic addition reactions. Formation of these reactive groups positions CreE as a promising candidate for biomedical and synthetic applications. Here, we present the catalytic mechanism of CreE and the identification of active site residues critical to binding L-aspartate, aiding in future enzyme engineering efforts. Steady-state analysis demonstrated that CreE is very specific for NADPH over NADH and performs a highly coupled reaction with L-aspartate. Analysis of the rapid-reaction kinetics showed that flavin reduction is very fast, along with the formation of the oxygenating species, the C4a–hydroperoxyflavin. The slowest step observed was the dehydration of the flavin. Structural analysis and site-directed mutagenesis implicated T65, R291, and R440 in the binding L-aspartate. The data presented describes the catalytic mechanism and the active site architecture of this unique FMO.

Introduction

Cremeomycin is a light-sensitive compound that has potent antitumor effects against murine leukemia L-1210 cells and has also displayed broad antimicrobial effects against both Gram-positive and Gram-negative bacteria and several fungal species.[1,2] Cremeomycin was first isolated in 1967 from *Streptomyces cremeus* by the Upjohn Company and in 1995 the chemical structure and physical properties were determined.[1,2] The structure features a novel diazocarbonyl functional group (Scheme 1A). The synthesis of diazocarbonyl functional groups has long been of interest for biomedical and synthetic applications because of their ability to serve as reactive intermediates in challenging organic synthesis reactions such as cycloadditions and C–H insertions.[3] Cremeomycin and other diazocarbonyl compounds have been successfully chemically synthesized, however, the syntheses utilize chemicals that are harmful to the environment and the yields are limited.[3–5] Therefore, the biosynthesis of cremeomycin presents an exciting opportunity to utilize enzymes from the biosynthetic pathway to synthesize cremeomycin and potentially other diazo-containing compounds in an environmentally friendly and efficient manner.

Recently, the biosynthetic pathway of cremeomycin from *Streptomyces cremeus* was elucidated (Scheme 1).[6] In this pathway, the diazo moiety has been proposed to be formed by a *N–N* bond between nitrite and 3-amino-2,4-dihydroxybenzoate, catalyzed by the ATP-dependent fatty acid–coenzyme A (CoA) ligase, CreM (Scheme 1A).[7] Nitrite formation was shown to occur from the reactions of a flavin-dependent monooxygenase (CreE) and a nitrosuccinate lyase (CreD) (Scheme 1B).[6,8] The formation of nitrite by these enzymes is also an opportunity to form a highly reactive functional group without the need for environmentally harmful chemicals or high temperatures.[9] The mechanisms of CreD and CreM have been previously studied and therefore, this work is focused on the characterization of CreE, an enzyme central to both nitro and diazo group formation.[7,10]

CreE is a recently identified member of the vast and diverse enzyme family called flavin-dependent monooxygenases (FMOs).[6,8] FMOs require a flavin prosthetic group in the form of flavin adenine dinucleotide (FAD) or flavin mononucleotide (FMN) to catalyze oxygenation reactions of a variety of substrates for many different biological purposes.[11,12] FMOs are divided into eight subclasses (A–H) based on their structure and mechanism. The structure of a homologous enzyme to CreE from *Streptomyces sp. V2* L-aspartate *N*-monooxygenase (SV2–NMO) shows that these enzymes are members of class B of the FMO family.[13] The structures of class B FMOs feature two Rossmann nucleotide binding folds, of which one is responsible for FAD binding and the other binds NADPH/NADP$^+$.[11] The kinetic mechanism can be divided into two parts: the reductive and oxidative-half reactions. The reduction of class B FMOs can take place in the absence of substrate, known as the "bold"

[a] Dr. S. B. Johnson, Dr. H. Valentino, Prof. P. Sobrado
Department of Biochemistry and Center for Drug Discovery
Virginia Tech
360 West Campus Drive, Blacksburg, VA, 24061 USA

[b] Prof. P. Sobrado
Department of Chemistry, Missouri University of Science and Technology,
Rolla, MO 65409
E-mail: psobrado@vt.edu

Supporting information for this article is available on the WWW under https://doi.org/10.1002/cbic.202400350

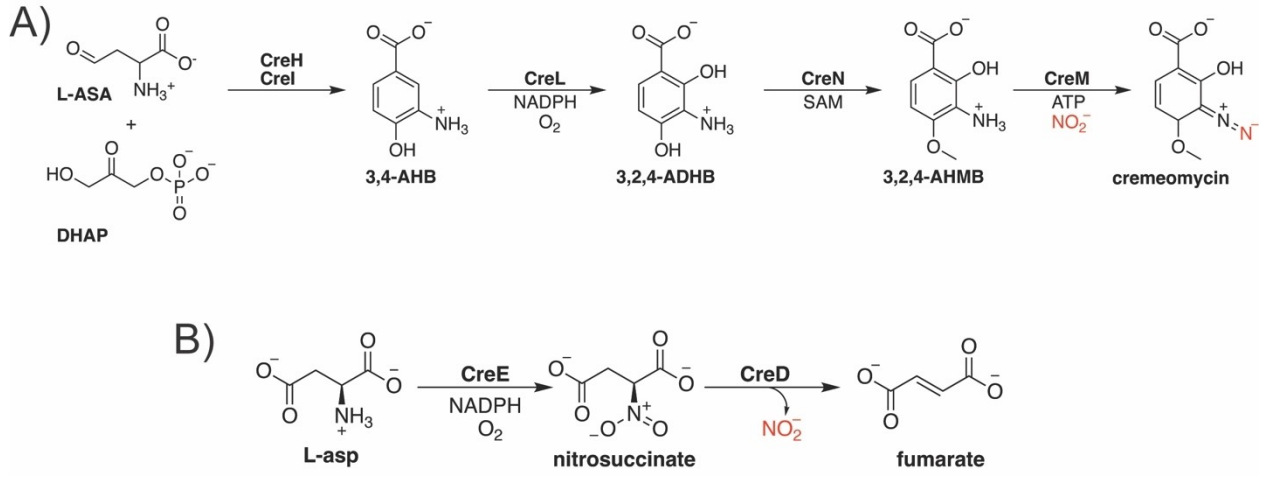

Scheme 1. Biosynthetic pathway of cremeomycin in *Streptomyces cremeus.* A) L-aspartate semialdehyde (ASA) and dihydroxyacetone phosphate (DHAP) are cyclized to 3-amino-4-hydroxybenzoate (3,4-AHB) by the class I aldolase homolog CreI and 3-dehydroquinate synthase II homolog CreH. The cyclization likely proceeds through the formation of a C–C bond formed by CreI. 3,4-AHB is hydroxylated by the flavin-dependent monooxygenase, CreL, to produce 3-amino-2,4-dihydroxybenzoate (3,2,4-ADHB). 3,2,4-ADHB is O-methylated by the SAM-dependent methyl transferase, CreN, producing 3-amino-2-hydroxy-4-methyloxybenzoate (3,2,4-AHMB). 3,2,4-AHMB is diazoated resulting from the nitrite and ATP-dependent reaction catalyzed by the fatty acid–CoA ligase, CreM, to cremeomycin. The nitrogen in the diazo group that originates from nitrite is shown in red. B) Nitrite is produced by the 6-electron oxidation of L-aspartate to nitrosuccinate by the flavin-dependent monooxygenase, CreE, and elimination of nitrite by the nitrosuccinate lysase, CreD, forming nitrosuccinate.

mechanism of flavin reduction.[12,14] After reduction, the $NADP^+$ is retained, which is a hallmark of class B.[14] In the oxidative-half reaction, the bound $NADP^+$ stabilizes the oxygenating intermediate, the C4a–hydroperoxyflavin, preventing the wasteful uncoupling of this intermediate to hydrogen peroxide.[14,15] Class B is further divided into four subclasses based on the substrate and reaction specificity: the flavin-containing monooxygenases, Baeyer-Villiger monooxygenases (BVMOs), nitrogen hydroxylating monooxygenases (NMOs), and YUCCAs.[11] CreE a member of the NMO subclass enzymes, which catalyze nitrogen oxidation reactions and are highly specific for their substrate.[11,16] However, CreE is an unusual member of this subclass, because the enzyme catalyzes three sequential hydroxylation reactions of L-aspartate to yield nitrosuccinate, in contrast to the typical single oxidation reaction of NMOs (Scheme 1B).[8,11,13,17]

Here we present the kinetic characterization of CreE. Steady-state kinetic studies demonstrated that CreE is stereospecific for L-aspartate and that the oxidation is highly coupled. Rapid-reaction kinetic analysis showed fast flavin reduction and C4a–hydroperoxyflavin formation steps and a slow flavin dehydration step. Multiple sequence alignment with related enzymes coupled with structural analysis of a CreE model and the crystal structure of SV2–NMO identified potential active site residues. Site-directed mutagenesis and biochemical characterization showed critical roles for T65, R291, and R440 in substrate binding and oxygenation. These findings lay the foundation for CreE as a promising candidate for enzyme engineering and chemoenzymatic biomedical applications.

Experimental Procedures

Materials

The gene encoding for CreE (UniProt ID: A0A0K2JL70) cloned into pMAL-c4x plasmid was obtained from Genscript Biotech (Piscataway, NJ). The gene encoding for *Tb*ADH (UniProt ID: P14941) cloned into pET-28a plasmid was also obtained from Genscript Biotech. Escherichia *coli* BL21(DE3) and OneShot TOP10 chemically competent cells were purchased from Invitrogen (Carlsbad, CA). All reagents were purchased from Research Product International (Mount Prospect, IL) unless otherwise stated. Glucose oxidase, d_8-2-isopropyl alcohol, fumarate, D-aspartate, and Amicon molecular weight cutoff centrifugal filters were obtained from Sigma Aldrich (St. Louis, MO). L-aspartate was purchased from Fisher Scientific (Hampton, NH). Protein purification was carried out on a Cytiva (Marlborough, MA) AKTA Start system using MBPTrap High Performance and HisTrap Fast Flow 5 mL columns. Sonication was carried out with a Fisher Scientific Sonic Dismembrator Model 500 (Hampton, NH). Enzyme activity was measured using a Hansatech Clark-type oxygen electrode system (Norfolk, UK) to measure oxygen consumption. Rapid-reaction kinetics were monitored using an Applied Photophysics (Surrey, UK) SX-20 stopped-flow instrument housed in a COY Laboratories (Grass Lake, MI) anaerobic chamber. All gas tanks were purchased from Airgas (Randor, PA). Data deconvolution was carried out using Applied Photophysics Pro-KIV software (Surrey, UK) and data analysis was performed using the Synergy Software (Reading, PA) program, Kaleidagraph and the GraphPad Prism software (Boston, MA).

Protein Expression and Purification

The pMAL-c4x-*CreE* plasmid was transformed into chemically competent *E. coli* BL21(DE3) cells. CreE was expressed as a N-terminal fusion to maltose binding protein (MBP) as described by Fox, et. al., 2009.[18] The cells were grown in autoinduction medium at 37 °C and 250 RPM until an optical density at 600 nm of 4.0 was reached. The temperature was lowered to 18 °C and cells were

grown overnight. The cells were harvested by centrifugation and stored at −70 °C until purification.

For protein purification, the cell pellet was thawed on ice and resuspended in 5 mL per gram of cells in Buffer A (50 mM potassium phosphate, pH 7.5, 300 mM NaCl, 10% glycerol). The solution was supplemented with 1 mM phenylmethylsulfonyl fluoride (PMSF), 25 μg/mL lysozyme, 10 μg/mL DNAse I, and 10 μg/mL RNAse and was stirred at 4 °C for 20 min. The cell suspension was sonicated at 70% amplitude for 15 minutes, with the pulse on for 5 seconds and off for 10 seconds. The lysate was centrifuged at 16,000 x *g* and 4 °C for 45 minutes to pellet the insoluble material and cell debris. The supernatant was loaded onto two-in tandem 5 mL MBPTrap columns equilibrated in Buffer A at 2.5 mL/min using an AKTA Start system. The columns were washed with Buffer A until the absorbance value decreased to baseline levels. CreE–MBP fusion was eluted using a in A over 15 column volumes at 5 mL/min and was collected in 5 mL fractions. The CreE–MBP fusion eluted between 25 mM and 50 mM maltose. Fractions were analyzed by SDS-PAGE for purity and fractions with pure protein were pooled. The protein was diluted to 5 mg/mL to avoid precipitation and was dialyzed overnight at 4 °C into 100 mM potassium phosphate, pH 7.5, 150 mM NaCl, 1 mM tris(2-carboxyethyl)phosphine–hydrochloride (TCEP–HCl), 10% glycerol (Buffer C). The MBP tag was cleaved by adding Tobacco Etch Virus (TEV) protease to the dialysis bag at a ratio of 1:30 (TEV: fusion protein).

To remove the MBP, TEV protease, and any uncleaved protein, the sample was loaded onto a 5 mL HisTrap column equilibrated in Buffer C at 2.5 mL/min. Cleaved CreE has a low affinity to the HisTrap column and was eluted and isolated from the TEV using a gradient of 0 to 100% of Buffer D (50 mM potassium phosphate, pH 7.5, 300 mM NaCl, 300 mM imidazole, 10% glycerol) over 15 column volumes at 5 mL/min and 5 mL fractions were collected (CreE elutes between 5–20 mM imidazole). Fractions were analyzed by SDS-PAGE for purity and fractions with pure protein were pooled. Pooled fractions were dialyzed for four hours at 4 °C into the storage buffer (100 mM potassium phosphate, pH 7.5, 150 mM NaCl, 1 mM TCEP–HCl, 10% glycerol). The protein was flash-frozen as 10 μL droplets and stored at −70 °C. The protein concentration was measured by Bradford assay and the FAD-bound extinction coefficient was calculated as previously described.[19,20]

Synthesis of (R)-[4-^{2}H-]-NADPH

For kinetic isotope effect studies NADPH and (*R*)-[4-^{2}H]-NADPH were synthesized as described by Jeong, et. al. with some modifications.[21] 5.5 mM $NADP^+$, 1 M d_8-2-isopropyl alcohol (for (*R*)-[4-^{2}H]-NADPH synthesis) or 1 M 2-propanol (for NADPH synthesis), and 2.5 μM of *Thermoanaerobacter brockii* alcohol dehydrogenase (expression and purification described below; *Tb*ADH) were added to 25 mM Tris–HCl, pH 9.0. The reaction was allowed to proceed for 20 minutes at 40 °C and was stirred at 125 RPM in an incubator until the A_{260}/A_{340} ratio reached a value of $\leq$2.8. The solutions were filtered with a 3 kDa Amicon molecular weight cut-off centrifugal filter to remove the enzyme. The filtrate was lyophilized to afford the products as light-yellowish powder. The product was stored at −70 °C and was resuspended in 100 mM potassium phosphate, pH 7.5, 100 mM NaCl immediately prior to usage.

*Tb*ADH was expressed in *E. coli* BL21(DE3) as a 6x His Tag fusion in pET-28a using the same procedures as described for CreE. *Tb*ADH was purified using Ni^{2+}–NTA chromatography. Cells were lysed using the same procedures as described for CreE in 25 mM Tris–HCl, pH 7.3, 300 mM NaCl, 5 mM imidazole, 0.1 mM TCEP–HCl. The insoluble proteins and cell debris were removed using the same procedures as described for CreE. *Tb*ADH was loaded onto two-in tandem HisTrap, 5 mL columns at 2 mL/min. The columns were washed with 10% of 25 mM Tris–HCl, pH 7.3, 300 mM NaCl, 300 mM imidazole, 0.1 mM TCEP–HCl, for 5 column volumes. *Tb*ADH was eluted using a gradient elution of to 100% 25 mM Tris–HCl, pH 7.3, 300 mM NaCl, 300 mM imidazole, 0.1 mM TCEP–HCl, over 15 column volumes and pure fractions were pooled as assessed by SDS-PAGE. The protein was dialyzed into a storage buffer of 25 mM Tris–HCl, pH 7.3, 100 mM NaCl, 0.05 mM $ZnSO_4$ overnight with stirring at 4 °C. The protein was flash frozen as 10 μL droplets and was stored at −70 °C.

Oxygen Consumption Assay

All oxygen consumption assays were performed using an Oxygraph + system from Hansatech Instruments (Norfolk, UK). Assays were performed in 100 mM potassium phosphate, pH 7.5, 100 mM NaCl (1 mL total volume). The concentration of CreE (and mutant enzymes) was 0.5 μM unless otherwise noted. All reactions were initiated by the addition of NADPH. In experiments where the NADPH concentration was varied (0.01–1 mM), L-aspartate was held constant at 20 mM. When L-aspartate was varied (0.075 mM–20 mM), NADPH was kept at 1 mM unless otherwise noted. For experiments where D-aspartate was varied (2.5 mM–100 mM), NADPH was also kept at 1 mM. When NADH was varied (0.25–4 mM), 1 μM enzyme was used and L-aspartate was held at 20 mM. For T65A, R291A, and R447A, 1 μM of enzyme was used to obtain rates above background at all concentrations tested. With T65A, R291A, and R440A, L-aspartate was varied at higher concentrations to reach saturation (10 mM–1000 mM). Eq. (1) was used to determine the turnover number (k_{cat}), and Michaelis-Menten constant (K_M). Reactions under saturating conditions were performed in the presence of 1 mg/mL catalase to determine the reaction coupling as previously described.[22]

$$\frac{v_0}{[E_T]} = \frac{k_{cat}[S]}{(K_M + [S])} \quad (1)$$

Rapid-Reaction Kinetic Analysis

The reductive and oxidative-half reactions of CreE were investigated using an Applied Photophysics SX20-stopped-flow spectrophotometer enclosed an anaerobic chamber. Oxygen was removed from the enzyme sample, buffer, and substrate stock as described previously.[17,23] NADPH was transferred directly to the chamber and resuspended in the anaerobic activity buffer (100 mM potassium phosphate, pH 7.5, 100 mM NaCl). For all stopped-flow experiments, the concentrations listed are after mixing. Flavin reduction was investigated by mixing various concentrations of NADPH (125–4000 μM) with 10 μM CreE at 5 °C. Kinetic isotope effect experiments were determined using 4 mM of (*R*)-[4-^{2}H]-NADPH and NADPH. Absorbance changes between 200–800 nm were recorded. The flavin reduction was monitored by measuring the decrease in absorbance at 448 nm was fit to Eq. (2) to obtain the observed rate constant of the fast phase (k_{red1}) and of the slow phase (k_{red2}). A_{448} is the absorbance at 448 nm, A is the amplitude of the phase, *t* is time, and C is the final absorbance at 448 nm. The observed rates obtained as a function of NADPH concentration were fit to Eq. (3), to determine the rate constant for flavin reduction (k_{red}) and dissociation constant (K_D) for NADPH.

$$A_{448} = C + A_1 e^{-(k_1 t)} + A_2 e^{-(k_2 t)} \quad (2)$$

$$k_{obs} = \frac{k_{red}[S]}{(K_D + [S])} \quad (3)$$

For the flavin oxidation experiments, reduced CreE was prepared by manually mixing 10 μM CreE with 15 μM NADPH. Saturated oxygenated buffer was prepared as previously described.[23] Oxidation was investigated at atmospheric oxygen concentrations (300 μM). Absorbance changes between 200–800 nm were recorded. Formation of the C4a–hydroperoxyflavin was monitored at 373 nm and traces were fit to Eq. (4) to obtain the observed rate constants (k_{OOH}). The flavin oxidation was monitored at 448 nm to obtain the k_1 for the decay and k_2 for the increase. In both of these equations, A_{nm} is the absorbance values at a specified wavelength, A_0 is the initial absorbance, and A_Δ is the amplitude of the absorbance change at a specified wavelength. In the absence of aspartate k_2 in Eq. 5 reports the value for k_{OX}, which is the decay of the C4a–hydroperoxyflavin. In the presence of aspartate, reports the value for k_{OH}, which is the decay of the C4a–hydroperoxyflavin. All data fitting was carried out with KaleidaGraph. Spectral deconvolution was carried out with a three-step model that accounted for the reduced enzyme, the C4a–hydroperoxyflavin, and the oxidized flavin.

$$A_{nm} = A_\Delta(1 - e^{-(k_{OOH}t)}) + A_0 \quad (4)$$

$$A_{nm} = A_{\Delta 1}e^{-(k_1 t)} + A_{\Delta 2}(1 - e^{-(k_2 t)}) + A_0 \quad (5)$$

Site-Directed Mutagenesis

All mutants of CreE were generated using the Q5 Site-Directed Mutagenesis Kit from New England Biolabs by following the instructions from the manufacturer. Plasmids containing the desired mutation were confirmed by Sanger DNA sequencing at the Genomic Sequencing Center in the Fralin Life Science Institute at Virginia Tech. All mutant enzymes were purified in the same manner as the wildtype and will be referred to as T65A, R291A, R440A, R443A, and R447A from hereon.

Bioinformatics and Structural Analysis

CreE was aligned to homologs and to other class B NMOs using MAFFT from the European Bioinformatics Institute.[24] The alignment was visualized by the Escript3.0 server.[25] The structural model of CreE was predicted using the AlphaFold2 ColabFold server.[26,27] The structure was validated using QMEAN from the Swiss Institute of Bioinformatics.[28] Structural alignment was conducted using the protein structure comparison service PDBeFold at European Bioinformatics Institute.[29] Visualization of all protein structures were conducted with PyMOL by Schrödinger.[30]

Results and Discussion

Protein Expression and Purification

Recombinant CreE was expressed as an N-terminal fusion to maltose-binding protein in *E. coli* BL21(DE3) cells using auto-induction media. The CreE–MBP fusion protein was purified using amylose affinity chromatography. CreE was cleaved from MBP by TEV protease and was isolated using Ni^{2+}–NTA chromatography. Cleaved CreE was isolated at a yield of 1.5 ± 0.1 mg of protein per gram of cell (Figure S1). The UV-visible spectrum of CreE displayed absorption peaks at 380 and 448 nm, indicating the protein was bound to a flavin cofactor (FAD) with 60 ± 5% incorporation (Figure S1). The extinction coefficient of the FAD bound CreE was calculated to be 12.5 $mM^{-1}\cdot cm^{-1}$.

Steady-State Kinetic Analysis

The steady-state kinetic parameters of CreE were determined using an oxygen consumption assay. A k_{cat} of 4.28 ± 0.07 s^{-1} and a K_M of 0.82 ± 0.06 mM were measured with L-aspartate, which are similar to previously reported values for homologous enzymes (Figure 1 & Table 1).[13,17] We observed little change on the k_{cat} value with D-aspartate but noted a ~23-fold increase in the K_M value, suggesting that CreE preferentially binds L-aspartate (Figure 1 & Table 1). A previous report showed that SV2–NMO was not active with D-aspartate by monitoring the rate of NADPH oxidation.[13] It is likely that an appropriate concentration of D-aspartate was not used to observe significant activity in this report.[13] We also measured the steady-state kinetic parameters with NADPH and NADH. Compared to NADPH, we observed a ~5.6-fold decrease in the k_{cat} value and ~39-fold increase in the K_M value with NADH (Figure 1 & Table 1). These findings indicate that CreE significantly prefers

Table 1. Steady-State Kinetic Results for the CreE Wildtype Enzyme.

Varied Substrate	Fixed Substrate	k_{cat} (s^{-1})	K_M (mM)	k_{cat}/K_M ($M^{-1}\cdot s^{-1}$)
L-aspartate	NADPH	4.28 ± 0.072	0.82 ± 0.06	5,200 ± 310
D-aspartate	NADPH	4.96 ± 0.120	19 ± 1.2	300 ± 10
NADPH	L-aspartate	4.51 ± 0.073	0.030 ± 0.001	150,000 ± 8,200
NADH	L-aspartate	0.810 ± 0.034	1.16 ± 0.091	700 ± 40
(*R*)-[4-^{2}H]-NADPH*	L-aspartate	2.35 ± 0.071	0.037 ± 0.002	66,000 ± 7,300
NADPH*	L-aspartate	4.68 ± 0.062	0.038 ± 0.002	122,000 ± 6,150

Conditions: 100 mM potassium phosphate, 100 mM NaCl, pH 7.5. Errors reported are from the data fitting analysis, except for the kinetic isotope effect, where the error is the standard deviation of three independent experiments. NADPH that was synthesized as described in the material and methods is indicated was an asterisk. *A $^D k_{cat}$ value of 2.0 ± 0.2 was calculated by determining the ratio between the k_{cat} values calculated with NADPH and (*R*)-[4-^{2}H]-NADPH. The errors were propagated from three independent experiments.

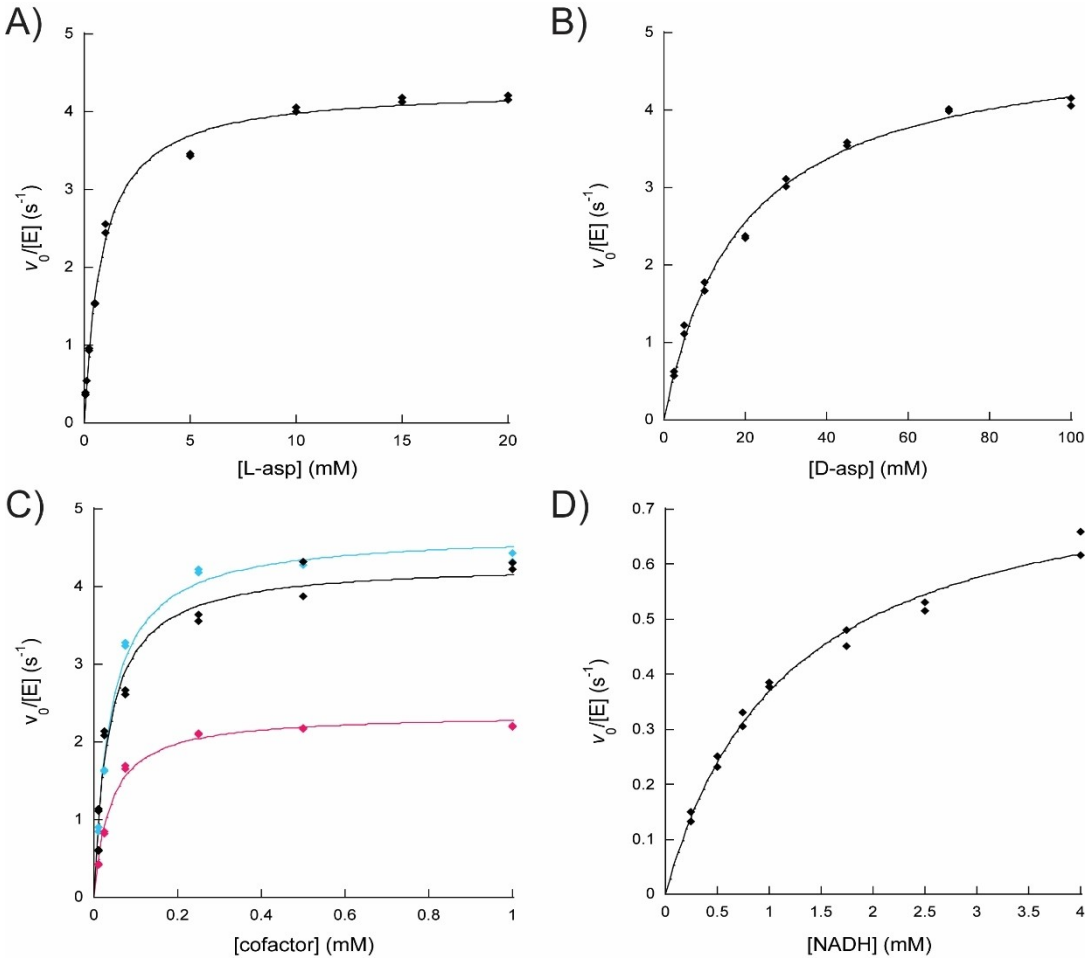

Figure 1. Steady-state kinetic analysis of CreE. Initial rates measured as a function of A) L-asp concentration (0.075–20 mM) and B) D-asp concentration (2.5–100 mM) were fit to Eq. (1). C) Initial rates measured with NADPH (black), synthesized NADPH (blue), and (*R*)-[4-^{2}H]-NADPH (pink) were fit to Eq. (1). All cofactors were tested between 0.01–1 mM. D) Initial rates measured with NADH (0.25–4 mM) were fit to Eq. (1).

NADPH over NADH for catalysis and binding, which is in agreement with a previous publication.[17]

FMOs typically couple oxygen activation to substrate hydroxylation, preventing the wasteful production of hydrogen peroxide known as uncoupling.[31–33] Because the oxygen consumption assay cannot distinguish between substrate hydroxylation and uncoupling, we performed reactions in the presence and absence of catalase at saturating conditions. Catalase will convert the hydrogen peroxide that is produced to molecular oxygen and water, lowering the oxygen consumption rate. At saturating conditions (0.5 μM CreE, 1 mM NADPH, 20 mM L-aspartate or 100 mM D-aspartate), we were unable to detect changes to the rate in the presence of catalase with L-aspartate, indicating the reaction is highly coupled. We observed that CreE is slightly less coupled with D-aspartate (84 ± 6 %). In contrast, a similar experiment with NADH showed that CreE is only 47 ± 3% coupled with this substrate, further supporting a significant preference for NADPH over NADH. To determine the kinetic isotope effect associated with hydride transfer, we measured the steady-state kinetic parameters with (*R*)-[4-^{2}H]-NADPH. The results show a kinetic isotope effect value on k_{cat} ($^D k_{cat}$) of 2.0 ± 0.2, indicating that hydride transfer is only partially rate-limiting and proceeds with pro*R* stereochemistry, which is consistent with several studies of related FMOs.[17,33–37] We also measured the effect on the initial rate with NADPH in the presence of various $NADP^+$ concentrations. The data showed a minimal effect on the k_{cat}, with increases in the K_M value, which is consistent with $NADP^+$ acting as a competitive inhibitor (Figure S2).[17,38] A K_I value for $NADP^+$ of 0.31 ± 0.07 mM was calculated (Figure S2).

Rapid-Reaction Kinetic Analysis

We studied the reductive and oxidative-half reactions of CreE using anaerobic stopped-flow spectroscopy. The reduction of CreE was measured by monitoring the bleaching of the absorbance at 448 nm at various NADPH concentrations (0.125–4 mM). The reduction occurred in two phases, where the fast phase (k_{red1}) was responsible for ~92% of the total amplitude change (Figure 2). The rate of reduction of the fast phase at 5 °C was 110 ± 3.5 s^{-1} and was dependent on the concentration of NADPH with a K_D value of 0.72 ± 0.05 mM, which agrees well with a report of a homologous enzyme, FzmM (Figure 2 &

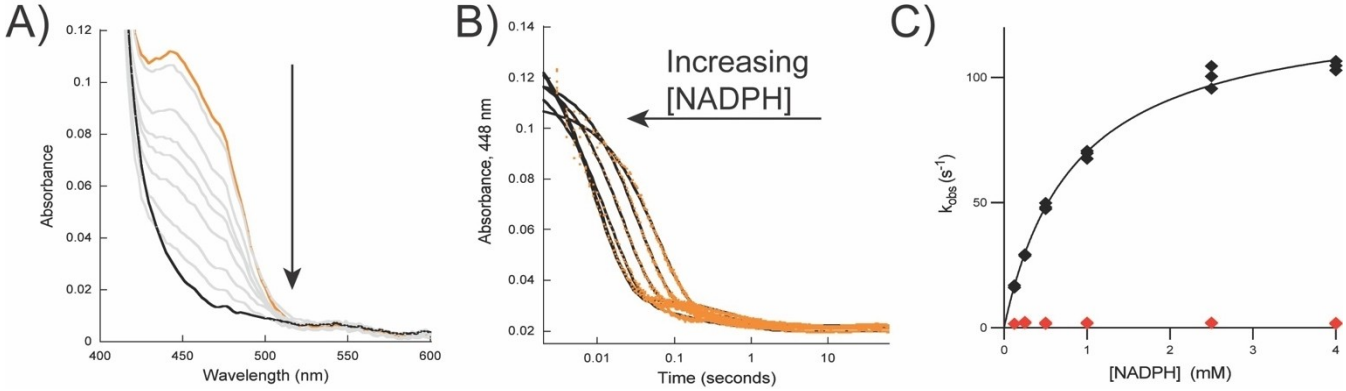

Figure 2. Reductive-half reaction of CreE. A) Reduction spectra of CreE at 4 mM NADPH over 30 seconds. The first recorded spectrum after mixing is in black and after 30 sec in orange. The spectra in gray are every 3 seconds. The arrow indicates the change in absorbance as time increases. B) Representative experimental traces at each NADPH concentration tested were fit to Eq. (2). The arrow indicates the direction of increase in the NADPH concentration. C) Fitting of the observed rates (fast phase (black), slow phase (orange)) at each NADPH concentration tested (0.125–4 mM) were fit to Eq. (3). The black dimonorange dimonds are the values obtains fro the slow phase of reduction.

Table 2. Reductive-Half Reaction Results.

Cofactor	k_{red1} (s^{-1})	k_{red2} (s^{-1})	K_D (mM)	k_{red1}/K_D ($M^{-1}\cdot s^{-1}$)
NADPH	110 ± 3.5	1.8 ± 0.16	0.72 ± 0.05	119,000 ± 4,000
R-[4-^{2}H]-NADPH*	26.8 ± 1.10	1.3 ± 0.19	N.A.	N.A.
NADPH*	119 ± 2.10	1.2 ± 0.23	N.A.	N.A.

Conditions: 100 mM potassium phosphate, pH 7.5, 100 mM NaCl and 5 °C. Errors reported are from the data fitting analysis, except for the kinetic isotope effect, which is the standard deviation of three independent experiments. NADPH synthesized following the procedures described in materials and methos are marked with an asterisk. *A $^D k_{cat}$ value of 4.4 ± 0.1was calculated by determining the ratio between the k_{cat} values calculated with NADPH and (*R*)-[4-^{2}H]-NADPH. The errors were propagated from three independent experiments.

Table 2).[17] We measured the kinetic isotope effect value on the reductive-half reaction using a saturating concentration of (*R*)-[4-^{2}H]-NADPH (4 mM). A kinetic isotope effect on the fast phase ($^D k_{red1}$) of 4.4 ± 0.1 was calculated, indicating that hydride transfer is the significant rate-limiting step within the reductive-half reaction. These findings also support that hydride transfer proceeds with pro*R* stereochemistry, as is the case with related FMOs.[17,33–37] The slow phase was not dependent on the NADPH concentration and was not isotope sensitive and likely originated from enzyme that was damaged during the degassing process (Table 2).

The oxidative-half reaction was monitored for the formation of the predicted oxygenating species, the C4a–hydroperoxyflavin (373 nm), and for the oxidation of the flavin (448 nm) in the presence and absence of L-aspartate at atmospheric oxygen concentrations (~300 μM). Deconvolution of the oxidation spectra in the absence of substrate showed the spectrum of the reduced flavin, the C4a–hydroperoxyflavin, and the oxidized flavin (Figure S3).[39] In the absence of L-aspartate, we observed that the C4a–hydroperoxyflavin forms fast upon mixing of the reduced enzyme with oxygen at a rate (k_{OOH}) of 54.5 ± 3.40 s^{-1} (Figure S3 & Table 3). We note that the spectrum of the C4a–hydroperoxyflavin has a small decrease in the ~448 nm region compared to the reduced spectra (Figure S3). Fitting of the rapid decrease at ~448 nm calculated a rate of 250 ± 20 s^{-1}. This indicates that this spectral change happens at a rate much faster than k_{cat} and may be related to changes in the active site that are required to form the C4a–hydroperoxyflavin. The rate of flavin oxidation (k_{OX}) in the absence of L-aspartate was slow at 0.088 ± 0.013 s^{-1} (Figure S3 & Table 3). These results demonstrate that the intermediate is stable and only uncouples to hydrogen peroxide in the absence of L-aspartate very slowly.[12–14,17,22,40]

Table 3. Oxidative-Half Reaction Results.

Conditions	k_{OOH} (s^{-1})	k_{OH} (s^{-1})	k_{OX} (s^{-1})
No substrate	54.5 ± 3.40	N.A.	0.088 ± 0.013
+ L-asp	46.6 ± 3.87	10.1 ± 0.120	N.A.

Conditions: 100 mM potassium phosphate, 100 mM NaCl, pH 7.5. Errors reported are the standard deviation of three replicates.

In the presence of L-aspartate, the rate of formation of the C4a–hydroperoxyflavin was similar to the rate obtained in the absence of L-aspartate (Figure 3 & Table 3). However, spectral deconvolution was not able to detect the C4a–hydroperoxyflavin completely independent from partially oxidized enzyme as indicated by the increase at ~448 nm (Figure 3). Furthermore, the rate constant for flavin dehydration (k_{OH}) is ~109-fold faster than k_{OX} (Figure 3 & S3 & Table 3). This is consistent with L-aspartate hydroxylation occurring very fast. We did observe a small decrease in the absorbance at the

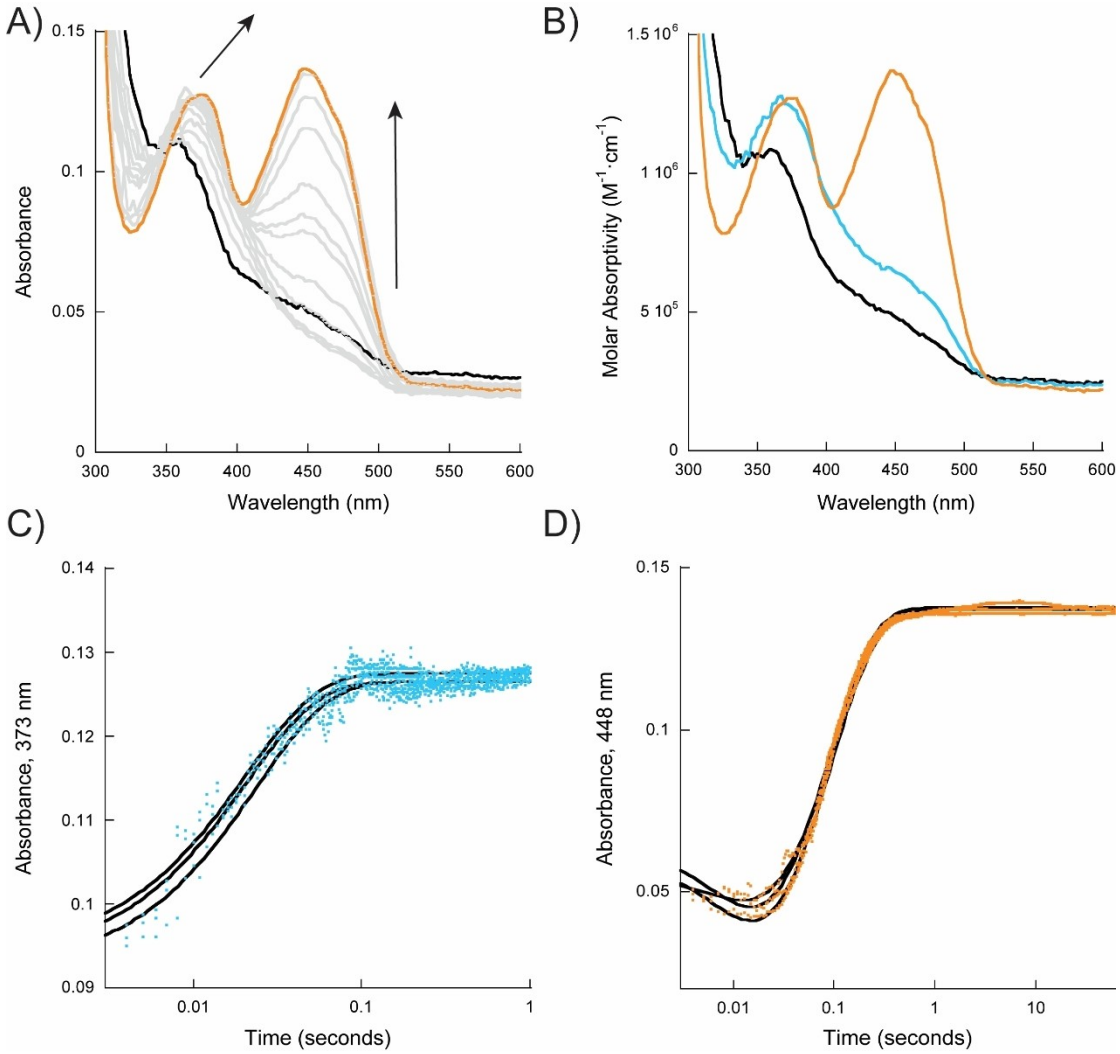

Figure 3. Oxidative-half reaction results in the presence of 20 mM L-aspartate. A) Spectra of 10 μM reduced CreE upon reaction with 300 μM oxygen over 60 seconds. The arrows indicate the direction of the absorbance changes as time increases. B) Deconvolution of the spectra from panel A. The predicted spectrum of the reduced flavin is in black, the C4a–hydroperoxyflavin is in blue, and the oxidized flavin is in orange. C) Experimental replicate traces (blue) at the 373 nm (absorbance corresponding of the C4a–hydroperoxyflavin) were fit to Eq. (4). D) Experimental replicate traces (orange) at the 448 nm (absorbance corresponding of the oxidized flavin) were fit to Eq. (5). In panels C&D, the black lines are the fittings to three independent replicates.

beginning of the traces at ~448 nm and determined a rate of $205 \pm 27\ s^{-1}$, which closely resembles the rate obtained for this decrease in the absence of L-aspartate, suggesting the substrate presence does not impact this process (Figure 3). Class B enzymes have been proposed to utilize a "cocked-gun" mechanism in which the C4a–hydroperoxyflavin is stabilized by the bound $NADP^+$ until the substrate is available for oxygenation to prevent the wasteful production of hydrogen peroxide.[15,39,41,42] The finding of a stable C4a–hydroperoxyflavin in CreE and the enhancement in the rate of flavin oxidation aligns well with the "cocked-gun" mechanism proposal (Table 3).

k_{OH} was the slowest step that was observed in the catalytic cycle, yet it is ~2-fold faster than the k_{cat} value measured for CreE (Tables 1 & 3).[38] This was also observed for FzmM, where k_{OH} was ~1.6-fold faster than the k_{cat} value.[17] Because CreE (and FzmM) catalyzes three rounds of oxidation, it is possible that flavin dehydration of the second or third oxidation step becomes slower and could correspond to the observed k_{cat} value. Alternatively, $NADP^+$ release might be the slow step in the catalytic cycle, however, given that NADPH must re-bind to kickstart the next reduction, this seems unlikely. Additionally, in the prototype NMO, SidA, $NADP^+$ release is fast, and the hydride transfer is the rate-limiting step, thus it is clear that the multiple oxidizing NMOs have different kinetic control.[15,35]

Structural Analysis

Recently, the crystal structure of SV2–NMO (55% identity to CreE) was solved with FAD and $NADP^+$ bound (Figure S4).[13] We generated a structural model of CreE using AlphaFold2 and compared it to the structure of SV2–NMO. The structure of SV2–NMO and the model of CreE align well (RMSD = 1.24 Å)

and both have two Rossmann-nucleotide binding folds, which is consistent with L-aspartate *N*-hydroxylases belonging to class B of the FMO family (Figure S4).[11] The SV2–NMO structure was solved with L-aspartate bound to the enzyme, but it is not bound in a conformation that is suitable for catalysis (Figure S5).

We performed the site-directed mutagenesis of several residues adjacent to the flavin, which were selected using knowledge of the binding site of the well-studied NMO, SidA, and recent work with SV2–NMO.[13,41,43] It was shown with SidA that upon formation of the C4a–peroxyflavin, the $NADP^+$ ribose 2′-OH donates a proton to form the C4a–hydroperoxyflavin.[41] This suggests that the C4a–hydroperoxyflavin forms between the flavin C4a and the $NADP^+$ ribose 2′-OH, indicating that the substrate atom that is to be hydroxylated needs to be in this vicinity. In the structure of SV2–NMO, $NADP^+$ is bound in the same conformation and location as that observed in SidA and other NMOs.[31,38,44] Thus, we considered that residues that were positively charged and/or could participate in hydrogen bonding within ~10 Å from the $NADP^+$ ribose 2′-OH and the pyrimidine ring of flavin could be involved in binding L-aspartate (Figure S5). Using these parameters, T65, R291, R440, and R443 were selected. These residues are conserved in other L-aspartate *N*-hydroxylases, however, they are not conserved in single oxidizing and well-studied NMOs (Figure S6). We mutated T65, R291, R440, and R443 to alanine to test their role in substrate binding (Figures S5 & S6). We also mutated R447 to alanine because it is found in an arginine-rich helix that is only conserved in multiple oxidizing NMOs and was previously proposed to facilitate substrate entry and binding alongside the other arginine residues in the helix, R440 and R443 (Figures S5 & S6).[13] Also of note, R291, R440, and R443 are conserved in other multiple oxidizing NMOs, PcxL and HpxL, which act on chemically similar substrates to L-aspartate (2-aminoethylphosphonate) (Figure S6).[45] It is likely that the substrates of PcxL and HpxL share similar active site interactions as with CreE.

Steady-State Kinetic Characterization of Mutant Enzymes

Each of the mutant enzymes were expressed and purified in the same manner as CreE with very similar results. We measured the steady-state kinetic parameters with L-aspartate for each of the mutant enzymes using the oxygen consumption assay. With T65A, we observed a ~2.5-fold decrease in the k_{cat} value and a ~28-fold increase in the K_M value (Figure S7 &Table 4). R440A gave similar results to T65A with ~1.8-fold decrease the k_{cat} value and a ~40-fold increase in the K_M value (Figure S7 &Table 4). Remarkably, R291A had a similar decrease in the k_{cat} value (~3-fold), but we also observed a ~290-fold increase in the K_M value (Figure S7 &Table 4). Together, these findings support that T65, R291, and R440 are important for binding L-aspartate and are key active site residues. With R443A, we observed a ~1.4-fold decrease in the k_{cat} with no change in the K_M value (Figure S7 & Table 4). R447A did not change the K_M value either, but a ~2.5-fold decrease in the k_{cat} value was observed (Figure S7 & Table 4). These results do not support a role for R443 or R447 in substrate binding. To test if the decreases in the k_{cat} value could be caused by a decrease in the reaction coupling we measured the initial rate constant in the presence of and in the absence of catalase with the oxygen consumption assay under saturating conditions. T65A and R447A were highly coupled, while R291A, R440A, and R443A were all very uncoupled (Table 4). A high degree of uncoupling could suggest that R291A, R440A, and R443A impact the stability of the C4a–hydroperoxyflavin and/or the ability to correctly orient L-aspartate in a position for optimal catalysis.

Conclusions

In this work we have described the catalytic mechanism of CreE and have identified residues involved in binding L-aspartate. The catalytic cycle of CreE begins with the binding of NADPH followed by the fast stereospecific pro*R* hydride transfer completing the reductive-half reaction (Scheme 2). In the oxidative-half reaction, the reduced flavin reacts with molecular oxygen to form the C4a–hydroperoxyflavin (Figures 3 & S3 & Scheme 2). In the absence of L-aspartate, the C4a–hydroperoxyflavin is stable and only eliminates to hydrogen peroxide very slowly (Figures S3 & Table 3). In contrast, in the presence of L-aspartate, oxidation is ~109-fold faster (Figures 3 & S3 & Table 3). After binding of L-aspartate, hydroxylation occurs via nucleophilic attack by the deprotonated amino group of L-aspartate to C4a–hydroperoxyflavin, forming *N*-hydroxy-aspartate and the C4a–hydroxyflavin (Scheme 2). The C4a–hydroxyflavin is dehydrated to regenerate

Table 4. Steady-State Kinetic Results with Mutant Enzymes and L-aspartate.

Enzyme	k_{cat} (s^{-1})	K_M (mM)	k_{cat}/K_M ($mM^{-1}\cdot s^{-1}$)	% Uncoupled
T65A	1.69 ± 0.040	22.8 ± 1.70	0.075 ± 0.005	5 ± 2
R291A	1.37 ± 0.020	235 ± 20.0	0.006 ± 0.001	87 ± 5
R440A	2.40 ± 0.030	32.9 ± 1.80	0.073 ± 0.003	61 ± 3
R443A	3.09 ± 0.060	0.88 ± 0.09	3.5 ± 0.30	44 ± 2
R447A	1.69 ± 0.040	0.82 ± 0.09	2.1 ± 0.21	N.D.

Conditions: 100 mM potassium phosphate, 100 mM NaCl, pH 7.5. Errors reported are from the data fitting, expect for the % uncoupled, where the error is the standard deviation of three independent experiments.

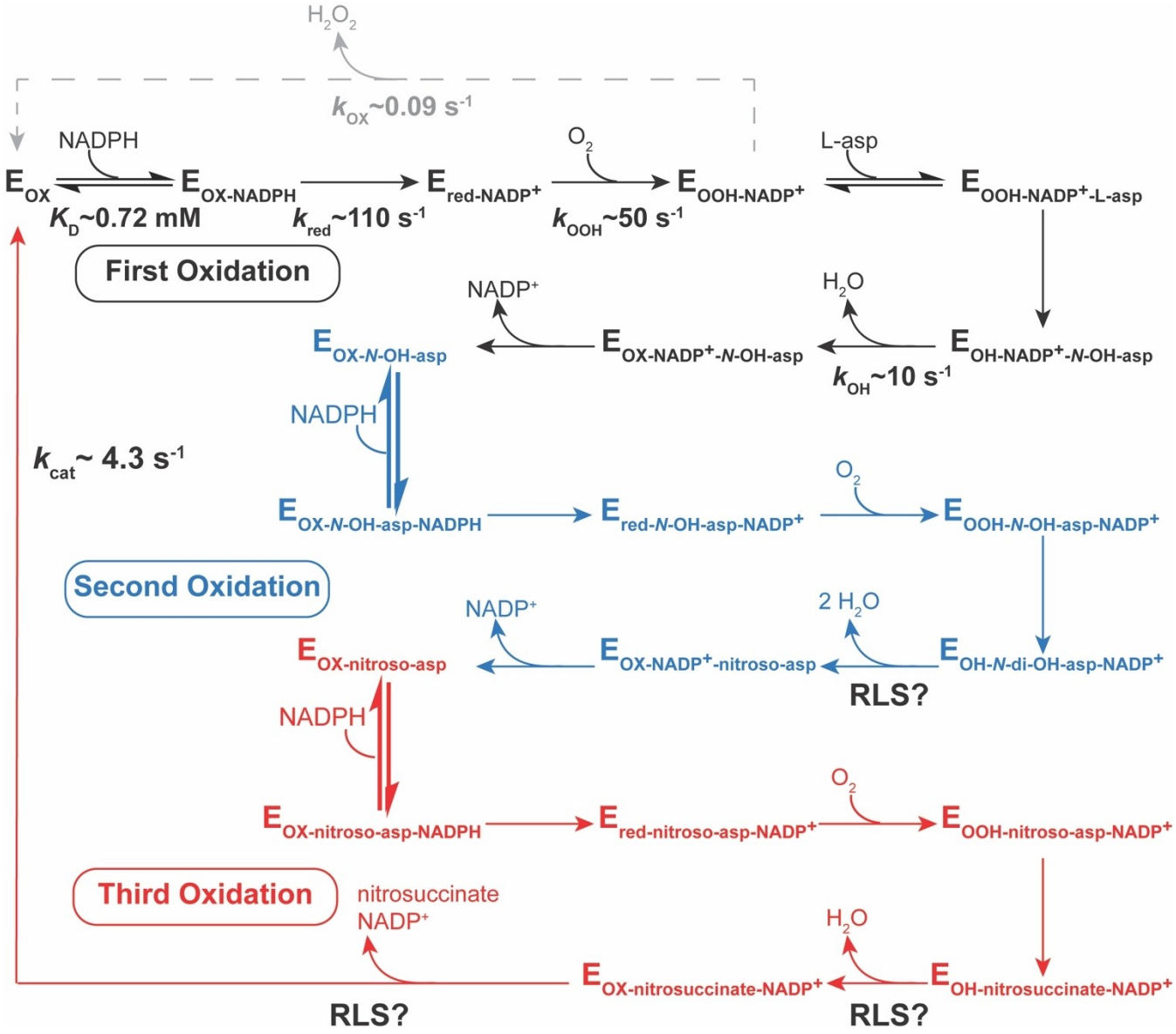

Scheme 2. Proposed reaction scheme of CreE. The first oxidation reaction begins with the binding of NADPH to the oxidized enzyme (E_{OX}), which is followed by the transfer of the pro*R* hydride from the C4 position of the NADPH nicotinamide to the flavin, generating the reduced enzyme in complex with $NADP^+$ ($E_{red\text{–}NADP+}$). The C4a–hydroperoxyflavin ($E_{OOH\text{–}NADP+}$) is formed upon the reaction of $E_{red\text{–}NADP+}$ with oxygen. The C4a–hydroperoxyflavin is stable, however it decays slowly in the absence of L-aspartate (dashed gray lines).$E_{OOH\text{–}NADP+}$ complexes with the L-aspartate, producing the enzyme-substrate complex ($E_{OOH\text{–}NADP+\text{–}L\text{-}asp}$). L-aspartate is then hydroxylated, forming *N*-hydroxy-aspartate and the C4a–hydroxyflavin ($E_{OH\text{–}NADP+\text{–}N\text{–}OH\text{-}asp}$). After flavin dehydration and the release of $NADP^+$, the first oxidation cycle is complete. The second oxidation is initiated by binding of NADPH to the $E_{OX\text{–}N\text{–}OH\text{-}asp}$. After hydride transfer, the $E_{red\text{–}NADP+\text{–}N\text{–}OH\text{-}asp}$ reacts with molecular oxygen to form the $E_{OOH\text{–}NADP+\text{–}N\text{–}OH\text{-}asp}$. After hydroxylation the $E_{OH\text{–}NADP+\text{–}N\text{-}di\text{–}OH\text{-}asp}$ would form. We propose that the *N*-di–hydroxy-aspartate is hydrolyzed to nitroso–aspartate, which serves as the substrate for the next round of oxidation. Following the same mechanism as the second oxidation, nitroso–aspartate is retained and upon release of $NADP^+$ the third oxidation can begin. NADPH binds the $E_{OX\text{–}nitroso\text{-}asp}$ and reduces the enzyme to form the $E_{red\text{–}NADP+\text{–}nitroso\text{-}asp}$. Molecular oxygen reacts with the $E_{red\text{–}NADP+\text{–}nitroso}$, forming the $E_{OOH\text{–}NADP+\text{–}N\text{–}OH\text{-}asp}$. After the third hydroxylation, the $E_{OH\text{–}NADP+\text{–}nitrosuccinate}$ complex is formed. Upon release of nitrosuccinate and $NADP^+$, the substrate-free, oxidized enzyme is regenerated (E_{OX}). Considering that flavin dehydration is the slowest step observed in the oxidation with L-aspartate, we propose that this step might be the rate-limiting step (RLS). Alternatively, the release of the final $NADP^+$ or nitrosuccinate could be or contribute to RLS.

the oxidized flavin and upon release of $NADP^+$, the second oxidation reaction takes place. As has previously been proposed, *N*-hydroxy-aspartate remains bound while awaiting the two next rounds of hydroxylation (Scheme 2).[13] While it is not clear what is the rate-limiting step, because flavin reduction, substrate hydroxylation, and flavin dehydration are faster than the k_{cat} value, it is possible that flavin dehydration step in the second or third oxidation reaction are the slowest steps (Scheme 2). Alternatively, resetting the protein after all three oxidation reactions by releasing nitrosuccinate and/or the final $NADP^+$ molecule could represent the rate-limiting step (Scheme 2).

The activity of CreE presents the opportunity to produce nitro functional groups in an environmentally friendly manner,

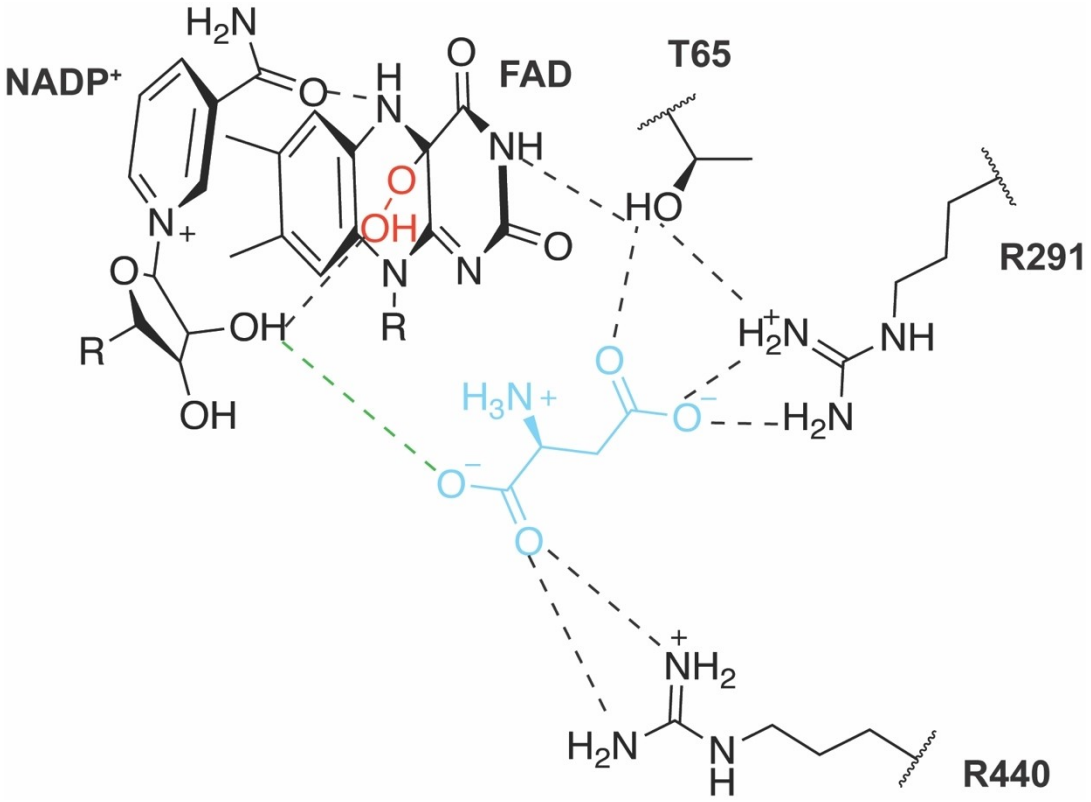

Figure 4. Proposed binding site of L-aspartate (blue). Predicted positions of residues involved in binding L-aspartate. T65 would remain in a similar position as observed in the structure of SV2–NMO and the model of CreE due to a hydrogen bond between the N3 of the flavin isoalloxazine and the hydroxyl group of the residue. The side chains of R291 and R440 would rotate towards the predicted substrate binding site to allow ionic interactions with the carboxyl groups of L-aspartate. R291 is predicted to interact with T65.

however, the substrate binding site was not known, hindering enzyme engineering efforts. Steady-state kinetic analysis of mutant enzymes showed that T65, R291, and R440 play a role in L-aspartate binding, while R443 and R447 do not (Figure 4, Figure S7 & Table 4). More studies will be required to determine if the decrease in the reaction coupling observed with R291A, R440A, and R443A is caused by improper substrate orientation and/or an increased instability of the C4a–hydroperoxyflavin. When considering that the position of L-aspartate should have the amino group in close proximity to the distal oxygen of the C4a–hydroperoxyflavin, it is clear that R291 and R440 are found in a position not optimal for binding L-aspartate in both the crystal structure of SV2–NMO and the model of CreE (Figure S5). Thus, rotation of the side chains must occur to accommodate binding to positions that have not yet been observed *in crystallo* (Figure 4). It is possible that the predicted flexibility of the active site residues in CreE is involved in resetting the protein after each hydroxylation step and could be unique to multiple oxidizing FMOs.

In summary, we have determined the catalytic mechanism of CreE with L-aspartate, which agrees with closely related enzymes.[13,17] Site-directed mutagenesis revealed residues that are involved in binding L-aspartate in the position in which catalysis takes place, facilitating future enzyme engineering for biomedical and synthetic applications to expand the substrate scope of this novel nitro-forming FMO.

Supporting Information

A file containing Figures S1–S7 is provided.

Acknowledgements

This work was supported by the U.S. National Science Foundation under the grant CHE 2003658. S.B.J also received financial support from the College of Agriculture and Life Sciences and the Department of Biochemistry as a member of the Graduate Teaching Scholars program at Virginia Tech.

Conflict of Interests

The authors declare no conflict of interest.

Data Availability Statement

The data that support the findings of this study are available in the supplementary material of this article.

Keywords: Natural Products · Flavin-Dependent Monooxygenase · Oxygenation · Kinetics · Mutagenesis

[1] J. N. McGuire, S. R. Wilson, K. L. Rinehart, *The Journal of Antibiotics* **1995**, *48*, 516–551. DOI: https://doi.org/10.7164/antibiotics.48.516.
[2] M. E. Bergy, T. R. Pyke, CREMEOMYCIN AND PROCESS FOR MAKING USA 1967.
[3] A. C. Burtoloso, C. B. Antonio, P. B. Momo, G. L. Novais, *An. Acad. Bras. Cienc.* **2018**, *90*, 859–893. DOI: 10.1590/0001-3765201820170768.
[4] L. M. Varley, C. J. Moody, *Synthesis* **2008**, *4*, 3601–3604, Article. DOI: 10.1055/s-0028-1083204.
[5] A. Ford, H. Miel, A. Ring, C. N. Slattery, A. R. Maguire, M. A. McKervey, *Chemical Reviews* **2015**, *115*, 18, 9981–10080. DOI: 10.1021/acs.chemrev.5b00121.
[6] A. J. Waldman, Y. Pechersky, P. Wang, J. X. Wang, E. P. Balskus, *ChemBioChem* **2015**, *16*, 2172–2175, Article. DOI: 10.1002/cbic.201500407.
[7] A. J. Waldman, E. P. Balskus, *J. Org. Chem.* **2018**, *83*, 7539–7546, Article. DOI: 10.1021/acs.joc.8b00367.
[8] Y. Sugai, Y. Katsuyama, Y. Ohnishi, *Nat. Chem. Biol.* **2016**, *12*, 73–75, Article. DOI: 10.1038/nchembio.1991.
[9] D. M. Badgujar, M. B. Talawar, P. P. Mahulikar, *Propellants Explos. Pyrotech.* **2016**, *41*, 24–34. DOI: https://doi.org/10.1002/prep.201500090.
[10] Y. Katsuyama, Y. Sato, Y. Sugai, Y. Higashiyama, M. Senda, T. Senda, Y. Ohnishi, *FEBS J* **2018**, *285:18*, DOI: 10.1111/febs.14429.
[11] M. M. Huijbers, S. Montersino, A. H. Westphal, D. Tischler, W. J. van Berkel, *Arch. Biochem. Biophys.* **2014**, *544*, 2–17. DOI: 10.1016/j.abb.2013.12.005.
[12] W. J. van Berkel, N. M. Kamerbeek, M. W. Fraaije, *J. Biotechnol.* **2006**, *124*, 670–689. DOI: 10.1016/j.jbiotec.2006.03.044.
[13] L. Rotilio, A. Boverio, Q. T. Nguyen, B. Mannucci, M. W. Fraaije, A. Mattevi, *J. Biol. Chem.* **2023**, *299*, 104904. DOI: 10.1016/j.jbc.2023.104904.
[14] B. A. Palfey, C. A. McDonald, *Arch. Biochem. Biophys.* **2010**, *493*, 26–36. DOI: 10.1016/j.abb.2009.11.028.
[15] C. Shirey, S. Badieyan, P. Sobrado, *J. Biol. Chem.* **2013**, *288*, 32440–32448. DOI: 10.1074/jbc.M113.487181.
[16] S. W. Chocklett, P. Sobrado, *Biochemistry* **2010**, *49*, 6777–6783. DOI: 10.1021/bi100291n.
[17] H. Valentino, P. Sobrado, *Biochemistry* **2021**, *60*, 2851–2864. DOI: 10.1021/acs.biochem.1c00512.
[18] B. G. Fox, P. G. Blommel, *Curr Protoc Protein Sci* **2009**, *5*, Unit-5.23. DOI: 10.1002/0471140864.ps0523s56.
[19] M. Oppenheimer, P. Michelle, M. P. Poulin, B. Myles, T. L. Lowary, R. F. Helm, P. Sobrado, *Arch. Biochem. Biophys.* **2010**, *502*, 31–38. DOI: https://doi.org/10.1016/j.abb.2010.06.035.
[20] K. S. Chapman, A. G. Reid, *Methods in molecular biology: Flavoprotein protocols*. Totowa, NJ: Springer: **1999**.
[21] S. S. Jeong, J. E. Gready, *Anal. Biochem.* **1994**, *221*, 273–277. DOI: S0003-2697(84)71411-4[pii]10.1006/abio.1994.1411.
[22] H. Valentino, A. C. Campbell, J. P. Schuermann, N. Sultana, N. Nazneen, G. Han, S. LeBlanc, J J. Tanner, P. Sobrado, *J. Biol. Chem.* **2020**, *295*, 11042–11055. DOI: https://doi.org/10.1074/jbc.RA120.014484.
[23] H. Valentino, P. Sobrado *Methods Enzymol.* **2019**, *620*, 51–88. DOI: 10.1016/bs.mie.2019.03.006.
[24] F. Madeira, M. Pearce, A. R. N. Tivey, P. Basutkar, J. Lee, O. Edbali, N. Madhusoodanan, A. Kolesnikov, R. Lopez, *Nucleic Acids Res.* **2022**, *50*, W276–W279. DOI: 10.1093/nar/gkac240.
[25] X. Robert, P. Gouet, *Nucleic Acids Res.* **2014**, *42*, W320–W324. DOI: 10.1093/nar/gku316.
[26] J. Jumper, R. Evans, A. Pritzel, T. Green, M. Figurnov, O. Ronneberger, K. Tunyasuvunakool, R. Bates, A. Žídek, A. Potapenko, et al., *Nature* **2021**, *596*, 583–589. DOI: 10.1038/s41586-021-03819-2.
[27] M. Mirdita, K. Schütze, Y. Moriwaki, L. Heo, S. Ovchinnikov, M. Steinegger, *bioRxiv* **2021**, DOI: 10.1101/2021.08.15.456425.
[28] P. Benkert, M. Biasini, T. Schwede, *Bioinformatics* **2010**, *27*, 343–350. DOI: 10.1093/bioinformatics/btq662.
[29] E. Krissinel, K. Henrick, *Acta Crystallogr. Sect. D* **2004**, *60*, 2256–2268. DOI: doi:10.1107/S0907444904026460.
[30] L. L. C. Schrodinger, The PyMOL Molecular Graphics System, Version 2.5. 2015.
[31] S. Franceschini, M. Fedkenheuer, N. J. Vogelaar, H. H. Robinson, P. Sobrado, A. Mattevi, *Biochemistry* **2012**, *51*, 7043–7045. DOI: 10.1021/bi301072w.
[32] C. Binda, R. M. Robinson, J. S. Martin del Campo, N. D. Keul, P. J. Rodriguez, H. H. Robinson, A. Mattevi, P. Sobrado, *J. Biol. Chem.* **2015**, *290*, 12676–12688. DOI: 10.1074/jbc.M114.629485.
[33] R. M. Robinson, P. J. Rodriguez, P. Sobrado, *Arch. Biochem. Biophys.* **2014**, *550–551*, 58–66. DOI: https://doi.org/10.1016/j.abb.2014.04.006.
[34] N. B. Beaty, D. P. Ballou, *J. Biol. Chem.* **1981**, *256*, 4611–4618. DOI: https://doi.org/10.1016/S0021-9258(19)69479–2.
[35] E. Romero, M. Fedkenheuer, S. W. Chocklett, J. Qi, Jun, M. Oppenheimer, P. Sobrado, *Biochim. Biophys. Acta Proteins Proteomics* **2012**, *1824*, 850–857. DOI: https://doi.org/10.1016/j.bbapap.2012.03.004.
[36] C. Ryerson, B. Cummings, P. David, C. Walsh, *Biochemistry* **1982**, *21*, 2644–2655. DOI: 10.1021/bi00540a011.
[37] S. Ghisla, V. Massey, In *EJB Reviews 1989*, P. Christen, E. Hofmann, Eds.; Springer Berlin Heidelberg, **1989**, pp 29–45.
[38] N. S. Lyons, A. N. Bogner, J. J. Tanner, P. Sobrado, *Biochemistry* **2022**, *61*, 2607–2620. DOI: 10.1021/acs.biochem.2c00493.
[39] R. Hille, S. M. Miller, B. Palfey, *Handbook of flavoproteins: Complex flavoproteins, dehydrogenases and physical methods*, **2013**. DOI: 10.1515/9783110298345.
[40] S. B. Johnson, K. Paasch, S. Shepard, P. Sobrado, *Archives of Biochemistry and Biophysics* **2024**, *754*, 109949. DOI: https://doi.org/10.1016/j.abb.2024.109949.
[41] R. Robinson, S. Badieyan, P. Sobrado, *Biochemistry* **2013**, *52*, 9089–9091. DOI: 10.1021/bi4014903.
[42] A. Alfieri, E. Malito, R. Orru, M. W. Fraaije, A. Mattevi, *Proc. Natl. Acad. Sci. USA* **2008**, *105*, 6572–6577. DOI: doi:10.1073/pnas.0800859105.
[43] R. Robinson, I. A. Qureshi, C. A. Klancher, P. J. Rodriguez, J. J. Tanner, P. Sobrado, *Arch. Biochem. Biophys.* **2015**, *585*, 25–31. DOI: 10.1016/j.abb.2015.09.008.
[44] J. Olucha, K. M. Meneely, A. S. Chilton, A. L. Lamb, *J. Biol. Chem.* **2011**, *286*, 31789–31798. DOI: 10.1074/jbc.M111.265876.
[45] M. N. Goettge, J. P. Cioni, K.-S. Ju, K. Pallitsch, W. W. Metcalf, *J. Biol. Chem.* **2018**, *293*, 6859–6868. DOI: 10.1074/jbc.RA118.001721.

Manuscript received: April 15, 2024
Revised manuscript received: May 17, 2024
Accepted manuscript online: May 22, 2024
Version of record online: July 3, 2024